UDK 666.3-135:669.715:539.375.6
Original scientific article/Izvirni znanstveni članek

ISSN 1580-2949
Mater. Tehnol.

INVESTIGATION OF THE WEAR-RESISTANCE CHARACTERISTICS OF ALUMINA-ZIRCONIA-TITANIA-COATED AL-6061 ALLOY FOR DIFFERENT PROCESSING PARAMETERS

ODPORNOST PROTI OBRABI TANKIH PREVLEK IZ MEŠANICE ALUMINIJ-CIRKONIJ-TITANOVEGA OKSIDA NA ZLITINI TIPA Al-6061, DOSEŽENE PRI RAZLIČNIH PROCESNIH PARAMETRIH

C. Suresh[1], D. R. P. Rajarathnam[2*], A. P. Sivasubramaniam[3], G. Saravanan[4]

[1,3]Paavai Engineering College, Department of Mechanical Engineering, Namakkal, India
[2]Paavai Engineering College, Department of Mechatronics Engineering, Namakkal, India
[4] Kongunadu College of Engineering and Technology, Department of Mechanical Engineering, Trichy Dt, India

Prejem rokopisa – received: 2024-11-23; sprejem za objavo – accepted for publication: 2025-02-18

doi:10.17222/mit.2024.1346

A ceramic coating is applied to the combustion chambers of diesel engines to reduce the heat transmission from the in-cylinder to the engine cooling system. Al alloy 6061 has moderate thermal stability and strength, which may not withstand the extreme heat and mechanical stresses generated in diesel engines. This necessitates protective coatings to enhance its wear resistance and thermal performance. Due to its strength and light weight, aluminum alloy 6061 is frequently utilized in commercial applications in the building, transportation, and related technical fields. For better qualities, coating powder made of alumina (Al_2O_3), zirconia (ZrO_2), and titanium dioxide (TiO_2) is applied to the engine cylinder's substrate. The specimens were coated using the plasma-spray method. To ensure strong adhesion, a 50-µm-thick bond coat of NiCrAlY was applied to the substrate before adding the top coat. The surface and cross-section of the specimens were analyzed using a Field-Emission Scanning Electron Microscope. X-ray diffraction analysis was performed to determine the structural and crystalline details. The performance of the coated specimens was then evaluated and compared to the uncoated ones. The specimen coated with a mixture of 35% Al_2O_3, 15% ZrO_2, and 50% TiO_2 demonstrated the best performance, with a wear rate of 0.03612 mm^3/Nm and a coefficient of friction of 0.357. This ceramic coating formulation is suggested for automotive parts that need enhanced wear and thermal resistance to extend their service life.

Keywords: ceramic coating, wear resistance, aluminum alloy, waer rate, thermal coating

Keramične prevleke se uporabljajo v zgorevalnih komorah dizelskih motorjev za zmanjšanje prenosa toplote z notranjosti valjev na hladilni sistem motorja. Zlitine na osnovi aluminija tipa Al 6061 imajo zmerno termično stabilnost in trdnost, ki pa ne prenesejo ekstremnih termičnih in mehanskih napetosti med delovanjem dizelskega motorja. Zato je potrebno uporabiti zaščitne prevleke, ki izboljšajo odpornost motorja proti obrabi in toplotnim obremenitvam. Zlitine tipa Al 6061 se zaradi svojih dobrih mehanskih lastnosti in majhne specifične gostote pogosto uporabljajo v gradbeništvu, transportu in drugih inženirskih področjih. Boljšo površinsko kakovost; i.e.: večjo trdoto in odpornost proti obrabi ter večjo termično stabilnost te vrste Al zlitin lahko dosežemo z nanosom aluminijevega oksida (Al_2O_3), zirkonijevega oksida (ZrO_2), in/ali titanovega oksida (TiO_2). To je še posebej uporabno v primeru motornih valjev (cilindrov) dizelskih motorjev. Avtorji v tem članku opisujejo napršavanje izbranih preizkušancev s pomočjo postopka napršavanja prašne mešanice v plazmi na površino preizkušancev. Avtorji so zato, da bi dosegli močno adhezijo najprej nanesli 50 µm plast NiCrAlY. Nato pa so nanesli še vrhnjo zaščitno oksidno (keramično) plast oziroma prevleko. Površino in presek izdelanih prevlek so avtorji analizirali s pomočjo vrstičnega elektronskega mikroskopa na emisijo polja (FE SEM; angl.: Field Emission Scanning Electron Microscope). Za določitev kristalne in fazne strukture so uporabili rentgenski difraktometer (XRD; angl.: X-ray diffraction analysis). Kakovost oziroma lastnosti prevleke so nato primerjali z neprevlečenim materialom. Vzorci prevlečeni z mešanico 35% Al_2O_3, 15% ZrO_2 in 50% TiO_2 so imeli najboljše lastnosti s hitrostjo obrabe 0,03612 mm^3/Nm in koeficientom trenja 0,357. Lastnosti keramične prevleke s to sestavo so dokaz, da je možno lastnosti (odpornost proti obrabi in termično stabilnost) osnovne zlitine, uporabljene za dele avtomobilskih motorjev, močno izboljšati in s tem zelo podaljšati njihovo življensko dobo oziroma uporabno dobo trajanja.

Ključne besede: keramična prevleka, odpornost proti obrabi, zlitine na osnovi aluminija, hitrost obrabe, termične prevleke

1 INTRODUCTION

Aluminum alloys are widely used in engineering applications due to their diverse beneficial properties. Among these, 6000 series aluminum alloys, such as Al6061, are favored for manufacturing cylinder blocks, crankcases, and pistons, offering significant weight reduction. Al6061 is particularly valued for its heat-treatment response, high toughness, resistance to corrosion, and mechanical integrity, making it ideal for medium- to high-strength structural uses. Components of an internal combustion engine like pistons and cylinder liners, often made from steel, cast iron, or aluminum alloys, are subjected to constant wear due to friction from continuous movement. These parts require a durable outer surface to resist abrasion and a flexible core to absorb energy. To enhance hardness and wear resistance, coatings are applied to these components, with ceramic coatings being

*Corresponding author's e-mail:
drprajamalathi@yahoo.co.in (D. R. P. Rajarathnam)

preferred for their superior durability and wear performance, contributing to longer component life. Alumina (Al_2O_3), zirconia (ZrO_2), and titanium dioxide (TiO_2) were chosen for their exceptional properties that meet the demands of internal combustion engine components. Al_2O_3 offers high hardness and wear resistance, ZrO_2 provides excellent thermal insulation and toughness, and TiO_2 enhances corrosion resistance and adhesion. Together, these materials create a durable, thermally stable coating that improves wear resistance, extends component life, and boosts engine efficiency by reducing heat loss. Ceramic coatings, like those made from alumina (Al_2O_3), zirconia (ZrO_2), and titanium dioxide (TiO_2), improve both thermal resistance and wear performance in automotive diesel engines. These coatings provide a thermal barrier that reduces heat transmission from the combustion chamber to the engine components, helping to maintain optimal operating temperatures and reduce thermal degradation. Simultaneously, their high hardness and low friction properties enhance wear resistance, minimizing abrasion and extending the service life of parts such as pistons, cylinder liners and valves. The combination of thermal insulation and wear resistance improves overall engine efficiency, reduces energy loss, and boosts component durability.

To assess the wear resistance of Al6061 plates using the pin-on-disc method in accordance with ASTM G99, ceramic oxides such as Al_2O_3 and ZrO_2-5CaO were applied through plasma coating. Studies on factors like porosity, microhardness, surface roughness, and microstructure revealed that rate of wear is impacted by applied load, porosity, splat morphology, and the microhardness of the coating. Scanning electron microscopy (SEM) was used to evaluate the effectiveness of the plasma coating.[1] Various thermal spray deposits on piston rings were also explored to minimize material degradation due to wear.[2] Research into nanostructured composite powders, including Al_2O_3, TiO_2, and ZrO_2, applied through plasma spraying, highlighted their properties in comparison to standard Al_2O_3-13 *w*/% TiO_2 coatings.[3] Additionally, low thermal conductivity ceramics were suggested for structural applications to better manage heat and temperature distribution, leading to improved performance.[4] The mechanical and wear characteristics of gradient coatings were examined, showing performance improvements.[5] Blends of Al_2O_3 + ZrO_2, ZrO_2 + 20 % Y_2O_3, and ZrO_2 + 8 % Y_2O_3 demonstrated superior resistance to wear in contrast to cast iron, often utilized for liners.[6] The article indicates that mullite's low coefficient of thermal expansion may lead to a bonding mismatch with the substrate, despite the material's favorable thermo-mechanical properties. For example, when mullite coating crystallizes between 1023 K and 1273 K, the volume contraction induced by this crystallization leads to cracking and de-bonding.[7] It was shown that mullite coating has a significantly reduced thermal cycle life above 1273 K compared to yttria (Y_2O_3) stabilized zirconia.[8] It has been noted that the improved wear properties of ceramics, along with reduced heat loss from the combustion chamber due to thermally insulated components, result in more heat energy being retained. This increase in available heat boosts the in-cylinder performance and increases the energy of exhaust gases, allowing for efficient use.[9]

A thermal barrier coating predominantly composed of zirconia was administered to diesel engine components.[10,11] Compared to an uncoated engine, the piston crown treated with plasma spraying demonstrated a 13.95 % improvement in thermal efficiency, a reduction of 9.84 % in gasoline used specifically for the brakes, and a drop of 6.02 % in mass fuel consumption. When self-mated instead of sliding against a metallic substrate, plasma-sprayed ZrO_2-8%Y_2O_3 (partially stabilized zirconia) showed improved wear resistance. Furthermore, the AA2024 composite's fly-ash-reinforced particle sliding-wear properties were investigated, and the results showed that the composite offered better wear resistance than the unreinforced base material. Additionally, it was found that the Al359 composite sample reinforced with boron carbide particles possessed a harder surface than the base material. The inclusion of a ceramic phase can increase the friction coefficient by as much as 20 % with weight addition. The resistance to wear of boron-carbide-reinforced composites was significantly improved.[12–15] The mechanical and physical properties of spark-plasma-sintered Ti and TiB_2 composite samples were analyzed, revealing that TiB_2 predominantly enhances mechanical qualities by refining the matrix grains.[16]

The efficacy of the components of a diesel engine, specifically the piston crown, cylinder head, and valves, was evaluated subsequent to the application of a 500-μm layer of mullite (60 % Al_2O_3 and 40 % SiO_2) over a 150-μm NiCrAlY bond layer. This resulted in a 16% drop in heat transmission to the coolant, a 22 % increase in heat transfer to the exhaust, and a 1.07 % reduction in specific fuel consumption.[17] A nanostructured Al_2O_3/TiO_2/ZrO_2 composite powder was prepared for plasma spraying; the ideal particle size was selected based on adhesion, powder density, and flowability to provide a robust binding. An Al6061 substrate covered with a combination of alumina and Y_2O_3-stabilized zirconia was tested for wear resistance.[18,19] The mechanical properties, such as strength, elongation, and hardness, of nano-reinforced castings utilizing Al_2O_3, TiO_2, and ZrO_2 exhibited substantial enhancement when fabricated in a semi-solid state at 600 °C. The improvement was noted with the incorporation of 2 *w*/% Al_2O_3 and 3 *w*/% TiO_2 or ZrO_2, while agitating at a velocity of 1500 min^{-1}.[20,21] The tribological performance of a piston ring can be enhanced by depositing a micron-thick layer of an appropriate material by the economical thermal spray coating technique. Integrating eco-friendly components into the coating composition with conventional ones enhances

sustainability.[22] Reports indicate that AISI 1024 materials are superior wear-resistant adherent protective oxide layer formation.[23] It was found that, compared to Yttria (Y_2O_3)-stabilized zirconia, a mullite coating has a shorter thermal cycle life at temperatures above 1273°C.[24] In AISI 1040 forged steel, the wear rate and coefficient of friction values reduced with TiC and WC coated specimen; however, the WC coating generated the lowest wear values. The TiC coating was most effective in reducing wear rates.[25] It was also looked into how nanostructured coatings derived from plasma-densified precursors exhibit markedly improved performance, as indicated by decreases in wear volume and mass loss.[26]

2 EXPERIMENTAL DETAILS

2.1. Materials

The inclusion of silicon and magnesium facilitates excellent mechanical properties such as machinability and weldability. The Al6061 alloy possesses moderate strength, excellent formability, and corrosion resistance. The Aluminium 6061 alloy exhibits lower wear resistance relative to other aluminium series and comprises a higher concentration of magnesium and silicon composites. It contributes to the hardening and fortification of materials.

2.2 Characteristics of powdered ceramic coating

Alumina (Al_2O_3) is a ceramic substance that is widely used in industry to increase hardness. Its hardness and chemical inertness make alumina (Al_2O_3) an ideal material for use in coatings. Moreover, a small amount of Al_2O_3 added to a coating material strengthens the bonds without reducing ductility. Due to its high heat conductivity and minimal thermal expansion, it may develop microscopic fissures when it melts and solidifies. Zirconium oxide (ZrO_2), commonly referred to as zirconia, is a durable ceramic utilized for the production of protective coatings. Electrical and thermal properties. When heated, zirconia undergoes phase transitions, which can be controlled by the doping process with small amounts of other compounds. Due to its low thermal conductivity, zirconia is a suitable material for thermal insulation coatings. Zirconia is used as a thermal barrier layer to reduce heat loss and thermal conductivity. Titanium dioxide (TiO_2), a chemically inert compound, protects the underlying material against degradation, discoloration, and fracture due to its capacity to absorb UV rays. The predominant surfaces that are white utilize TiO_2.

2.3 Thermal Plasma Deposition

Thermal Plasma Deposition employs a high-temperature heat source to melt and accelerate small particles onto a pre-treated substrate. Upon collision, these molten particles undergo rapid cooling and solidification via heat transfer to the substrate, resulting in the formation of a lamellar layer. Thermal spray techniques have been employed for numerous years to deposit multilayer coatings for diverse applications, including resistance to wear, heat insulation, biological compatibility, and bio-functionality. **Figure 1** presents a schematic representation of the coating layers along with their corresponding thicknesses.

Plasma spraying of the Al6061 alloy is commonly employed in the production of components for internal combustion engines, including pistons and cylinder liners. Consequently, Al6061 plates with dimensions of 30 mm × 3 mm × 3 mm are fabricated and exposed to several ceramic coatings for examination. The specimens are evaluated for dimensional precision, surface quality, and cleanliness to eliminate any dust or impurities. The selected ceramic coating can endure temperatures, rendering them appropriate because of their analogous reactive properties. The micro-scale geometry of the substrate functions as a layer interface between the alloy and the ceramic materials.

2.4 Microstructure Characterization and Mechanical Properties

A Scanning Electron Microscope (SEM) is a sophisticated electron microscope that generates high-resolu-

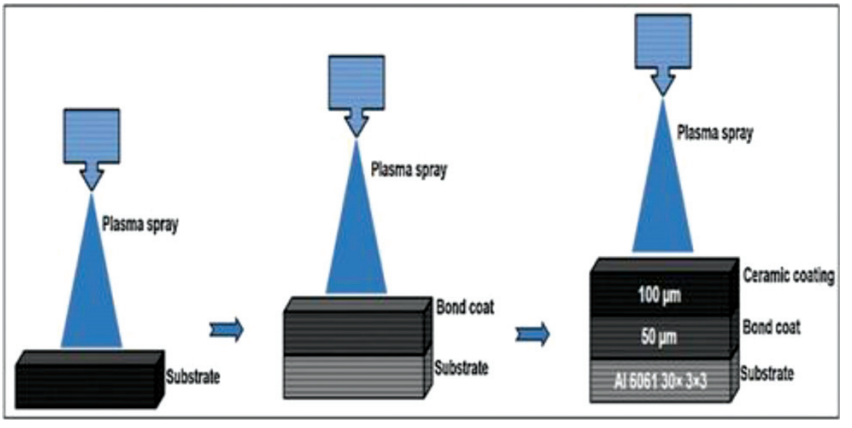

Figure 1: Coating layers and their thicknesses

tion images of a specimen's surface. In contrast to traditional optical microscopes, SEM employs a concentrated beam of electrons instead of light to generate images. X-Ray Diffraction (XRD) spectra were obtained to examine the crystallographic and structural orientation of the specimens. The X-ray diffraction profile of the coated specimen has a significant peak for Al, the primary alloy component, along with separate peaks for Al_2O_3, ZrO_2, and TiO_2. No peaks indicative of contaminants were observed in the spectra. Energy-Dispersive X-ray Spectroscopy (EDX) is employed to examine the elemental composition of a substance.

2.5. Pin-On-Disc Wear Testing Method

A Pin-On-Disc tribometer applies pressure from a small pin into a flat, rotating disc specimen, resulting in a circular wear pattern. This configuration is employed to examine the wear and friction properties of materials exclusively under sliding conditions. The revolving disc serves as the sliding contact surface, while the specimen may be either a disc or a pin. Various pin shapes may be utilised. A practical method termed "ball on disc" utilizes a spherical contact area composed of materials often encountered in daily life, like tungsten carbide, bearing steel, or alumina (Al_2O_3).

2.6 Hardness Measurements

Hardness is a material's resistance to plastic deformation caused by indentation. Hardness is occasionally used to denote a material's resistance to abrasion or scratching. It can sometimes be substituted by relatively swift and uncomplicated hardness assessments. Hardness may be assessed from a small sample of material without causing damage.

2.7 Optimization Technique

The input wear parameters for the specimen that showed the greatest wear resistance were optimized. Further research was conducted using Taguchi's L9 design for trials, single objective optimization using S/N ratio computation, and ANOVA to identify the impact of each component.

3 RESULTS AND DISCUSSION

This study aims to evaluate the effectiveness of ceramic coating systems in enhancing the structural characteristics of components of an internal combustion engine, including pistons and cylinder liners, to extend their operational lifespan.

3.1 Wear Analysis of Coating Samples

The wear rate of S1 exhibits a fast increase over the time periods from 21 s to 103 s (wear rate escalation: 0.00856 mm³/Nm to 0.003467 mm³/Nm), after which it decelerates, displaying only steady small increases until the conclusion (peaking at 0.004898 mm³/Nm). **Figure 2** illustrates the wear rates of the specimens: S1, S2, S3, S4, and S5. The wear curve of S2 exhibits a dramatic increase in rate of wear from 0.0015 mm³/Nm to 0.0030 mm³/Nm during the interval of 21 s to 41 s, after which the pattern stabilizes, demonstrating gradual increases until the conclusion of the cycle, culminating in a maximum wear rate of 0.0079 mm³/Nm. In comparison to S1, S2 exhibits a consistently higher wear rate from the commencement to the conclusion of the interval cycle.

The wear rate values derived from the wear test tests for the various proportionate combinations (S1, S2, S3, S4, and S5) are illustrated in **Figure 3**, which displays the wear rates of the samples: specimens S1, S2, S3, S4, and S5. The wear rate of S2 exhibits a sharp increase over the time periods from 21 s to 103 s (wear rate increase: 0.00675 mm³/Nm to 0.00712 mm³/Nm), after which it decelerates, demonstrating progressive small increments until the conclusion (culminating at 0.007625 mm³/Nm).

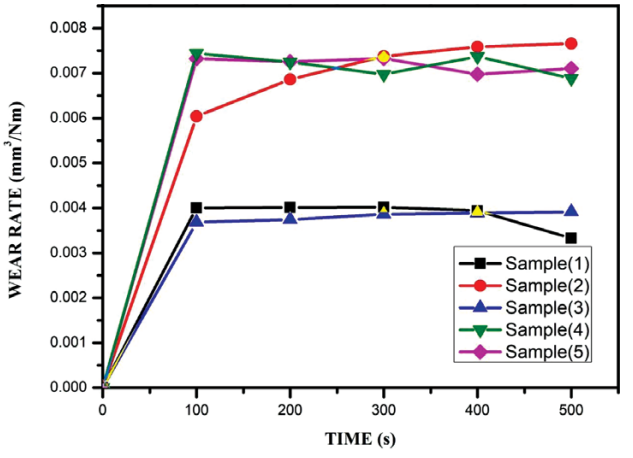

Figure 2: Schematic of coating layers and 10 N thickness load

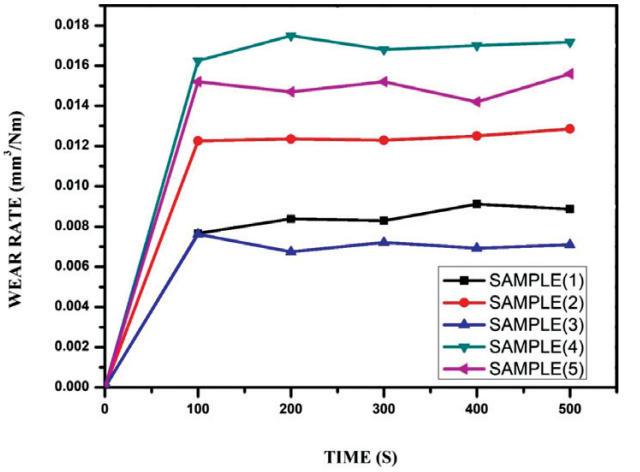

Figure 3: Schematic of coating layers and their thickness load 20 N

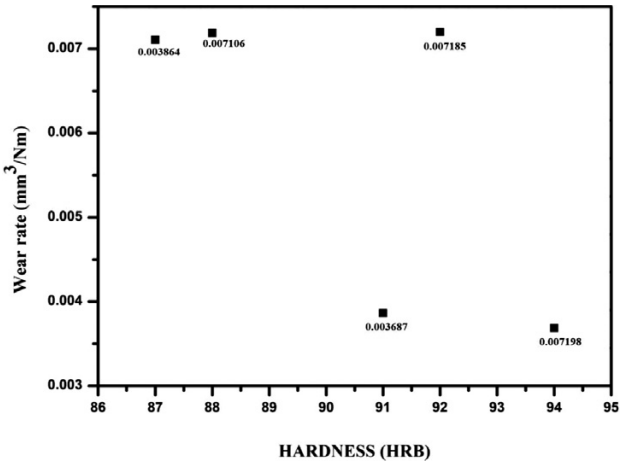

Figure 4: Schematic of wear rate and Harness –10 N

The wear curve of S2 exhibits a significant increase in rate of wear from 0.015 mm³/Nm to 0.030 mm³/Nm during the interval of 21 s to 41 s, after which the pattern stabilises, demonstrating progressive increments until the conclusion of the cycle, culminating in a maximum wear rate of 0.079 mm³/Nm. Compared to S1, S2 has a consistently higher wear rate from the commencement to the conclusion of the interval cycle.

The hardness values derived from the hardness test tests for the various proportionate combinations (S1, S2, S3, S4, and S5) are illustrated in **Figure 4**, which depicts the wear rates of the samples: specimens S1, S2, S3, S4, and S5. The hardness rate of S2 exhibits a dramatic increase over the time periods from 21 s to 103 s (hardness rate rise: 0.007106 mm³/Nm to 0.007198 mm³/Nm), after which the rate decelerates, displaying only steady, minor increments until the conclusion (maximum of 0.007106 mm³/Nm at the end). The hardness graph of S2 exhibits a dramatic increase between the 21st and 41st seconds.

The values derived from the hardness tests for the various proportionate combinations (S1, S2, S3, S4, and S5) are illustrated in **Figure 5**, which depicts the wear rates of the samples: specimens S1, S2, S3, S4, and S5. The hardness rate of S2 exhibits a sudden increase during the interval from 21 s to 103 s (hardness rate rise: 0.012448 mm³/Nm to 0.012334 mm³/Nm), after which the rate of increase diminishes, resulting in gradual, minor increments until the conclusion (maximum of 0.012448 mm³/Nm at the end). The hardness graph of S2 exhibits a dramatic increase throughout the interval from 21 s to 41 s.

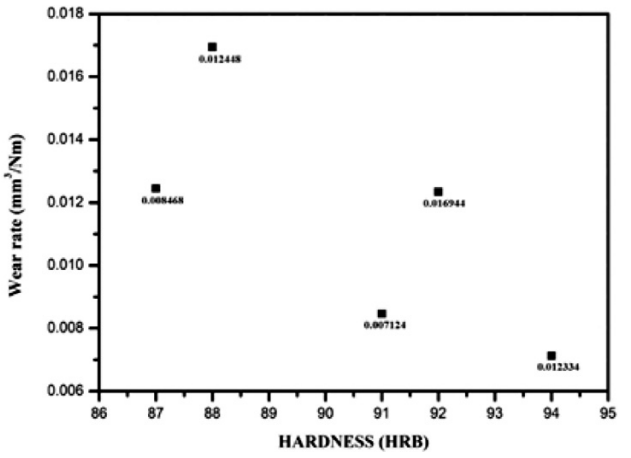

Figure 5: Schematic of wear rate and Harness –20 N

3.2 Characterization studies

3.2.1 Microstructure study results

Scanning electron microscopy with energy-dispersive X-ray spectroscopy (SEM/EDX) is the most prominent and often employed surface-examination technology. It utilizes a concentrated scanning electron beam to generate high-resolution, precisely defined pictures of surface topography. Scanning Electron Microscopy (SEM) produces intricate, high-resolution pictures by projecting a concentrated electron beam onto a surface and capturing secondary or backscattered electron signals. Furthermore, an Energy-Dispersive X-Ray Analyzer (EDX or EDA) can yield quantitative compositional data and facilitate elemental identification.

3.2.2 Material's composition and structure

Scanning electron microscopy (SEM) coupled with energy-dispersive X-ray spectroscopy (EDX) is the most

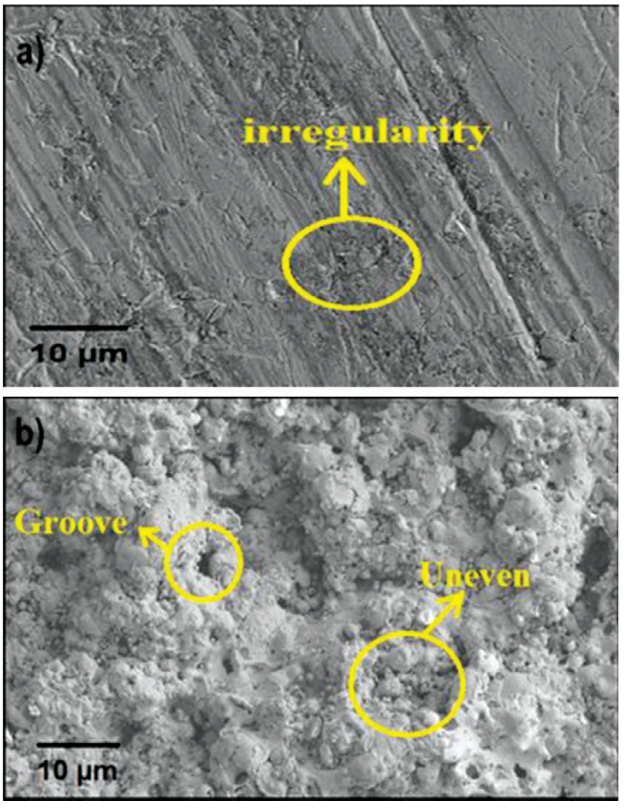

Figure 6: Schematic of SEM: a) uncoated Al-6061 substrate, b) coated Al-6061 substrate

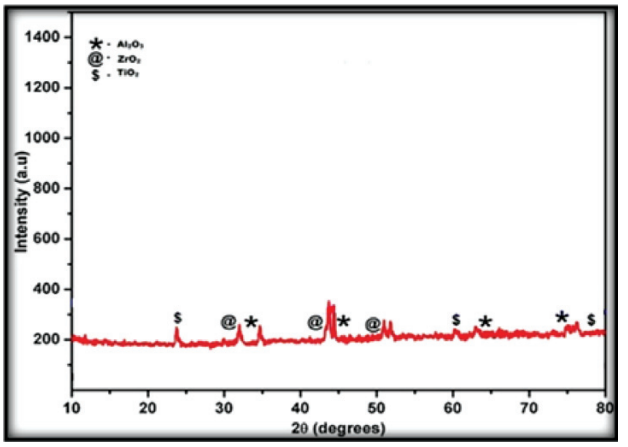

Figure 7: Schematic of XRD

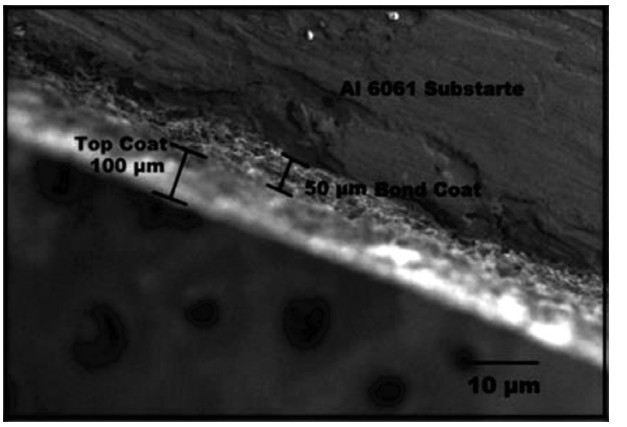

Figure 9: Schematic of FESEM

common surface-examination technology. A focused scanning electron beam is employed to generate high-resolution, precisely defined pictures of surface topography. Scanning Electron Microscopy (SEM) produces intricate, high-resolution pictures of materials by focusing a concentrated electron beam over the surface and detecting secondary or backscattered electron signals. Quantitative compositional data and elemental identification can be acquired utilizing an Energy-Dispersive X-ray Analyzer (EDX). X-ray diffraction (XRD) is utilized to examine the structural and crystallographic characteristics of the produced materials. The testing results indicated a significant enhancement in the tribological and mechanical capabilities of Al-6061 MMC compared to Al-6061 alloy. Notwithstanding their advantageous physical and mechanical properties, the aluminium alloys underperformed in certain high-performance and high-temperature applications. In the future, academic researchers will utilize this review article to identify the optimal permutations and combinations of reinforcements, along with optimized process parameters, for synthesizing various aluminum-based alloys. The mechanical properties of Al-6061 MMC are slightly enhanced with the inclusion of particle reinforcements. Photomicrographs of Al-6061 MMC microstructural behaviour demonstrated continuous interfacial bonding with homogeneity as shown in **Figure 6** and **Figure 7**. EDX spectrum and scanning electron microscopic (SEM) images for samples that are not coated. Following the completion of wear tests on the samples, all the SEM images are captured. The sectional view of the test specimen captured using FE-SEM shown in **Figure 9** highlights the applied bond coat and top coat layers. Plasma-spray coating was utilized to apply the bond coat and ceramic top coat to the substrate, with thicknesses of 50 µm and 100 µm, respectively. The coating is evenly dispersed throughout the specimen. The surface examination of the coating **Figure 8** indicates wear on the top coat, predominantly composed of a ceramic layer. The SEM examination verifies that the bond-coat and top-coat thicknesses, applied via plasma spraying, are 50µm and 100µm, respectively, for the S3 specimen.

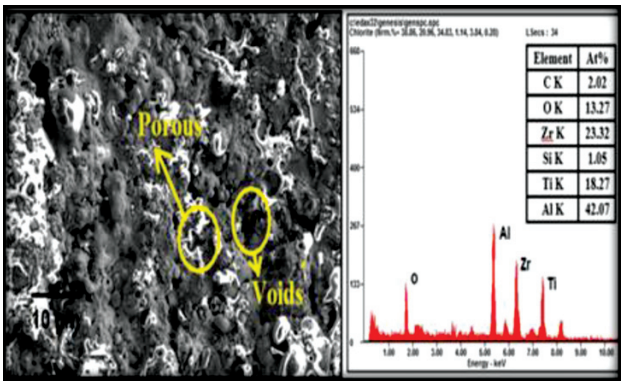

Figure 8: Schematic of EDX

3.3 Taguchi experimental studies

The experimental plan was structured using the Taguchi design approach, incorporating two factors at two levels and one factor at four levels, as shown in **Table 1**. This method delineates the variables for analysis and allocates their respective levels. The levels denote the precise values of the elements, organized in a mixed array with 16 rows – one column at four levels and two columns at two levels – resulting in a total of 15 degrees of freedom. Factors and their interactions are designated to these columns. The experimental results are shown in **Figure 10** and **Figure 11**, subsequently transformed into a signal-to-noise (S/N) ratio via the Taguchi method.

Table 1: Design factors used in experiment

Design Factors	Unit	Levels		
		1	2	3
Load (L)	N	10	15	20
Speed (N)	min^{-1}	500	600	700
Sliding Distance (SD)	m	1000	1500	2000

Lower is the better characteristic: S/N = –10 log 1/n (Σy^2)

Table 2: Orthogonal array mixed L9 of Taguchi

Experimental No.	Load (N)	Speed (min^{-1})	Sliding distance (m)	Wear rate (mm^3/Nm)
1	10	500	1000	0.1277
2	10	600	1500	0.1317
3	10	700	2000	0.1293
4	15	500	1000	0.03618
5	15	600	1500	0.0766
6	15	700	2000	0.0839
7	20	500	1000	0.0304
8	20	600	1500	0.0386
9	20	700	2000	0.0430

The wear rate decreases noticeably as the load increases from 10 N to 20 N. The wear rate varies from 0.1277 mm^3/Nm to 0.1317 mm^3/Nm at 10 N, but it dramatically drops to between 0.0304 mm^3/Nm and 0.0430 mm^3/Nm at 20 N, suggesting that the coatings are more effective in preventing wear at higher loads, as shown in **Table 2**. Increasing the speed results in a modest increase in wear rate when the load remains constant, albeit this effect is not as strong as the load itself. For instance, at 15 N, the wear rate increases from 0.03618 mm^3/Nm to 0.0839 mm^3/Nm as the speed increases from 500 min^{-1} to 700 min^{-1}. Furthermore, longer sliding distances typically result in a slight increase in wear rate; however, this impact becomes more noticeable at lower weights, such 10 N. Overall, as the loads are increased, the coatings' wear resistance gets better; nevertheless, as speed and sliding distance increase, it gets slightly less. Load is the most important element, with higher loads producing a noticeable reduction in wear rate.

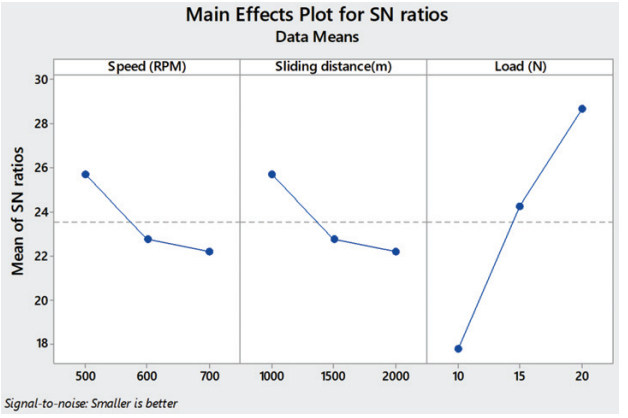

Figure 10: Plot diagram of SN ratios

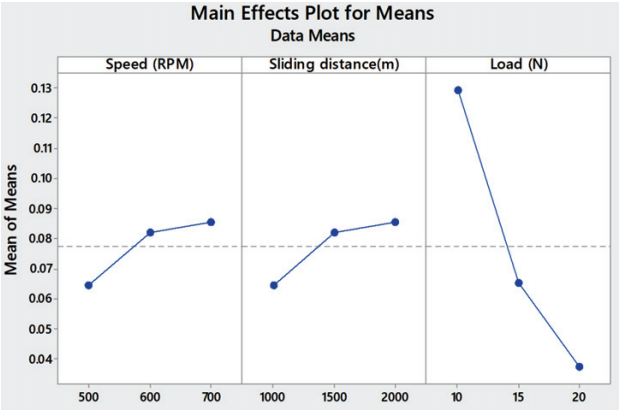

Figure 11: Schematic of Means

4 CONCLUSIONS

The wear characteristics of Al6061, frequently utilized for piston and cylinder liners in internal combustion engines, are evaluated to contrast them with newly introduced ceramic coatings. Al6061 specimens were coated with Al_2O_3 ceramic layers to perform wear testing and assess their resistance to wear. The Thermal Plasma Deposition process can result in high porosity, residual stress, and uneven coatings, affecting the performance of the Al alloy 6061. Excessive coating thickness may lead to cracking or delamination, while insufficient thickness may fail to provide adequate wear and thermal protection. These factors can compromise the coating's durability and functionality. The findings indicate that specimens coated with both system A and system B had enhanced wear resistance relative to the untreated specimens. Subsequent examination employed SEM micrographs and hardness assessments, while XRD measurements validated the structural integrity of the produced materials. The inquiry resulted in the subsequent conclusions.

1. The Scanning Electron Microscopy (SEM) study of the coating systems reveals that the thermal stresses induced during the spraying process are the primary source of micro cracks in the coating. The length of the substrate exposure to the plasma flame influences the dimensions of these micro cracks.

2. An increase in coating thickness correlates with a marginal rise in both porosity and surface roughness.

3. The XRD examination indicates that the fabricated coating systems have experienced a phase change, with tetragonal ZrO_2 and α-Al_2O_3 constituting the two predominant phases across all coating systems.

4. The rise in the coefficient of friction is primarily due to debris generated during three-body abrasion. The coefficients of friction and wear are significantly affected by the applied load. Initially, abrasion induces wear, and upon contact of the bond coat with the disc, material loss transpires via adhesion. The use of α-Al_2O_3 and ZrO_2 renders these coating systems appropriate for applications necessitating wear and thermal resistance, exemplified by cylinder liners in internal combustion engines.

5. The wear resistance of the coatings improves at higher loads, but tends to degrade with increased speed and sliding distance. Load is the most critical factor affecting the wear rate, as higher loads result in a substantial decrease in wear rate. Finally, it confirms that opti-

mizing the load parameter can lead to better wear resistance for the α-Al_2O_3 and ZrO_2 coatings.

Acknowledgement

The research work was supported by my father Mr M. Chinnusamy and my spouse Mrs.+ S. Saranya. Special thanks to Professor Dr K. K. Ramasamy and Dr M. Premkumar from Paavai Engineering College, Namakkal, India, for their valuable help.

5 REFERENCES

[1] N. Krishnamurthy, M. S. Murali, P. G. Mukunda, Tribological behavior of plasma sprayed Al_2O_3 and ZrO25CaO coating son Al-6061 substrate, Journal of High Temperature and Processes, 29 (**2010**), 111–126

[2] H. Hu, L. Mao, S. Yin, H. Liao, C. Zhang, Wear-resistant ceramic coatings deposited by liquid thermal spraying, Ceramics International, 48 (**2022**), 33245–33255

[3] Ahn Hyo-Sok, Kim Jang-Yun and Lim Dae-Soon, Tribological behaviour of Plasma sprayed zirconia coatings, Wear, 203 (**1977**), 77–87

[4] K. Ramachandran, V. Selvarajan, P.V. Ananthapadmanabhan, K. P. Sreekumar, Microstructure adhesion microhardness abrasive wear resistance and electrical resistivity of the plasma sprayed alumina and alumina titania coatings, Thin Solid Films, 315 (**1999**), 144–152

[5] A. Uzun, I. Cevik, M. Akcil, Effects of thermal barrier coating on turbocharged diesel engine performance, Surface and Coatings Technology, 116 (**1999**), 505–507

[6] T. Hejwowski, A. Weroński, The effect of thermal barrier coatings on diesel engine performance, Vacuum, 65 (**2002**), 427–432

[7] R. Soltani, H. Samadi, E. Garcia, T. Coyle, Development of Alternative Thermal Barrier Coatings for Diesel Engines, SAE Technical Paper, 2005-01-0650, doi:10.4271/2005-01-0650

[8] A. Skopp, N. Kelling, M. Woydt, L. M. Berger, Thermally sprayed titanium sub oxide coatings for piston ring / Cylinder liners under mixed lubrication and dry running conditions, Wear, 262 (**2007**), 1061–1070

[9] Y. Wang, S. Jiang, M. Wang, S. Wang, T. Danny Xiao, P. R. Strutt, Abrasive wear characteristics of plasma sprayed nanostructured alumina/titania coatings, Wear, 237 (**2000**), 176–185

[10] I. Taymaz, The effect of thermal barrier coatings on diesel engine performance, Surface and Coatings Technology, 201(**2007**), 5249–5252

[11] H. Wu, Y. Jin, A. R. Nicoll, G. Barbezat, Friction and wear of a plasma sprayed Al_2O_3-40%ZrO_2 cast iron system, Wear, 176 (**1997**), 49–60

[12] K.-H. Habig, Wear behaviour of surface coatings on steel, Tribology International, 22 (**1989**), 65–73

[13] Y. Guilmard, J. Denape, J. A. Petit, Friction and wear thresholds of alumina chromium steel pairs sliding at high speeds under dry and wet conditions, Tribology International, 26 (**1993**), 29–39

[14] A. Mohammadzadeh, A. Sabahi Namini, M. Azadbeh, A. Motallebzadeh, On the physical and mechanical properties of spark plasma sintered pure Ti and Ti-TiB composite, Materials Research Express, 5 (**2018**), 14–20

[15] P. Ramaswamy, S. Seetharamu, K. B. R. Varma, K. J. Rao, Thermal shock characteristics of plasma sprayed mullite coatings, Journal of Thermal Spray Technology, 7 (**1998**), 497–500

[16] Y. Yang, D. Yan, Y. Dong, X. Chen, L. Wang, Z. Chu, Preparing of nanostructured Al_2O_3–TiO_2–ZrO_2 composite powders and plasma spraying nanostructured composite coating, Vacuum, 96 (**2013**), 39–45

[17] N. Krishnamurthy, M. S. Prashanthareddy, H. P. Raju, H. S. Manohar, A study of parameters affecting wear resistance of aluminum and yttria stabilized zirconia composite coatings on Al -6061 substrate, International Scholarly Research Network, 12 (**2012**), 1–13

[18] WangYou, Jiang Stephen, Wang Meidong, Wang Shihe, Thermal shock characteristics of plasma sprayed mullite coatings, Wear, 237 (**2000**), 176–85

[19] Y. Liu, E. Fischer Traugott, A. Dent, The effect of thermal barrier coatings on diesel engine performance, Surf Coat Technol, 167 (**2003**), 68–76

[20] I. S. El-Mahallawi , A. Yehia Shash, A. Eid Amer, Nano reinforced Cast Al-Si Alloys with Al_2O_3, TiO_2 and ZrO_2 Nanoparticles, Metals, 5 (**2015**), 802–821

[21] H. Wu, Y. Jin, Friction and wear of a plasma sprayed Al_2O_3-40%ZrO_2 cast iron system, Wear, 176 (**1994**), 49–60

[22] R. S. Sonia, N. M. Walia, Suri, Sumit Chaudhary, A. Tyagi, Potential applications of thermal spray coating for I.C. engine tribology: A Review, Journal of Physics: Conference Series, 2021, 1950: 012041, doi:10.1088/1742-6596/1950/1/012041

[23] D. Pereira, J. Gandra, J. Pamies Teixeira, R. M. Miranda, Wear behaviour of steel coatings produced by friction surfacing, Journal of Materials Processing Technology, 214 (**2014**), 2858–2868

[24] P. N. Shrirao, A. N. Pawar, Experimental investigation on performance of single cylinder diesel engine with mullite as thermal barrier coating, Journal of Mechanical Engineering and Technology, 3 (**2011**), 45–54

[25] D. R. P. Rajarathnam, M. Jayaraman, Investigation of the wear behaviour of an AISI 1040 forged steel shaft with plasma-spray ceramic-oxide coatings for sugar-cane mills, Mater. Tehnol., 51 (**2017**), 95–100

[26] F. Marra, L. Baiamonte, C. Bartuli, M. Valente, Tribological Behaviour of Alumina-Titania Nanostructured Coatings Produced by Air Plasma Spray Technique, Chemical Engineering Transactions, 47 (**2016**), 127–132